Earth and Planetary Science Letters

Supporting Information for

Upper mantle and mantle transition zone thermal and water content anomalies beneath Northeast Asia: Constraints from receiver function imaging of the 410 and 660 km discontinuities

Muchen Sun[a,b,c], Stephen S. Gao (E-mail:sgao@mst.edu)[c], Kelly H. Liu[c], Xiaofei Fu[a]

[a] College of Earth Science and Research Institute of Unconventional Oil and Gas, Northeast Petroleum University, Daqing, Heilongjiang 163318, China

[b] State Key Laboratory of Marine Geology, Tongji University, Shanghai 200092, China

[c] Geology and Geophysics Program, Missouri University of Science and Technology, Rolla, Missouri 65409, USA

Contents of this file

The columns of Table S1 are:
1). Lon: longitude of the center of the circular bin
2). Lat: Latitude of the center of the circular bin
3). d410: Apparent depth of the d410 in km
4). d410_SD: Standard deviation of the d410 depth in km
5). d660: Apparent depth of the d660 in km
6). d660_SD: Standard deviation of the d660 depth in km
7). MTZ: Apparent MTZ thickness in km
8). MTZ_SD: Standard deviation of MTZ thickness in km
9). RFs: Number of receiver functions

Table S2 (uploaded as a separate EXCEL file): Mean d410 and d660 depths and MTZ thickness for the sub-regions. Table S2a is based on the IASP91 model, Table S2b shows the corrected depths and thickness using the model of Lu et al. (2019), and Table S2c is the same as Table S2b but using the Chen et al. (2017) model.

The columns in Table S2 are:
1). Area: Name of the divided area
2). d410: Mean d410 depth in km

3). d410_SD: Standard deviation of the d410 depth in km
4). No. of bins: Number of circular bins in the area for the d410
5). d660: Mean d660 depth in km
6). d660_SD: Standard deviation of the d660 depth in km
7). No. of bins: Number of circular bins in the area for the d660
8). MTZ: Mean MTZ thickness in km
9). MTZ_SD: Standard deviation of MTZ thickness in km
10). No. of bins: Number of circular bins in the area for MTZ thickness

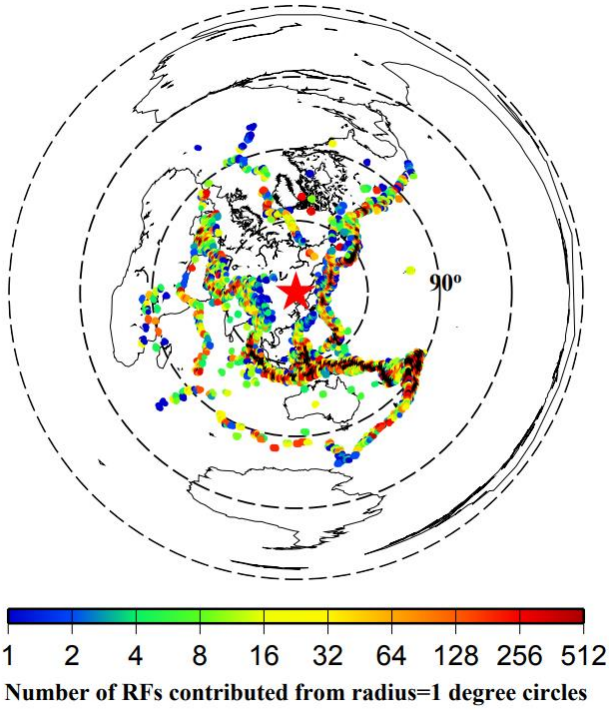

Figure S1. Spatial distribution of earthquake source areas. Each dot represents a radius = 1° circular area. The distance between neighboring circles is 1°. The color of the dot represents the number of used RFs originated from earthquakes in the circle. The radius of the concentric dashed circles centered at the central part of the study area (star) indicates the epicentral distance.

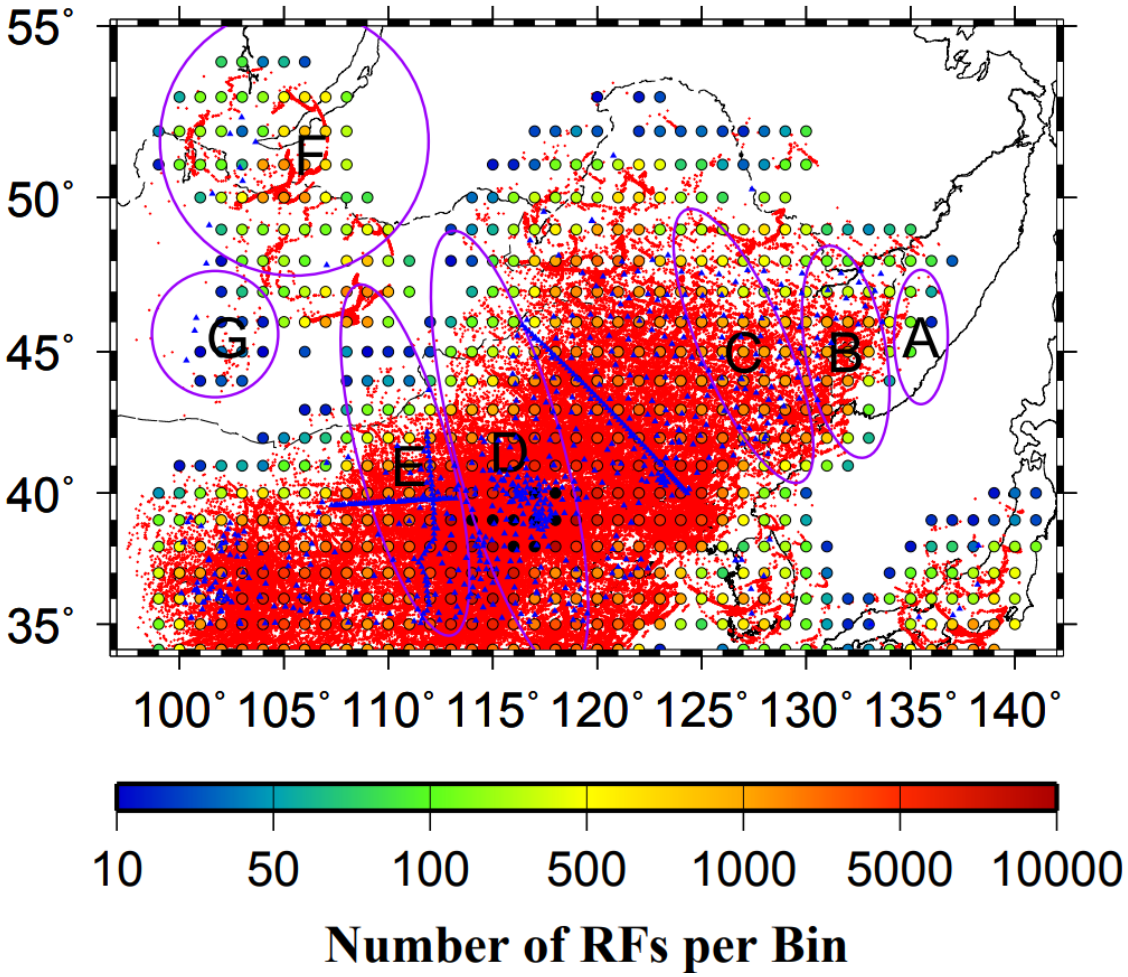

Figure S2. The red dots are ray-piercing points of P-to-s conversions at the depths of 535 km. The color of the circles represents the number of the RFs per bin. The blue triangles are seismic stations used in this study.

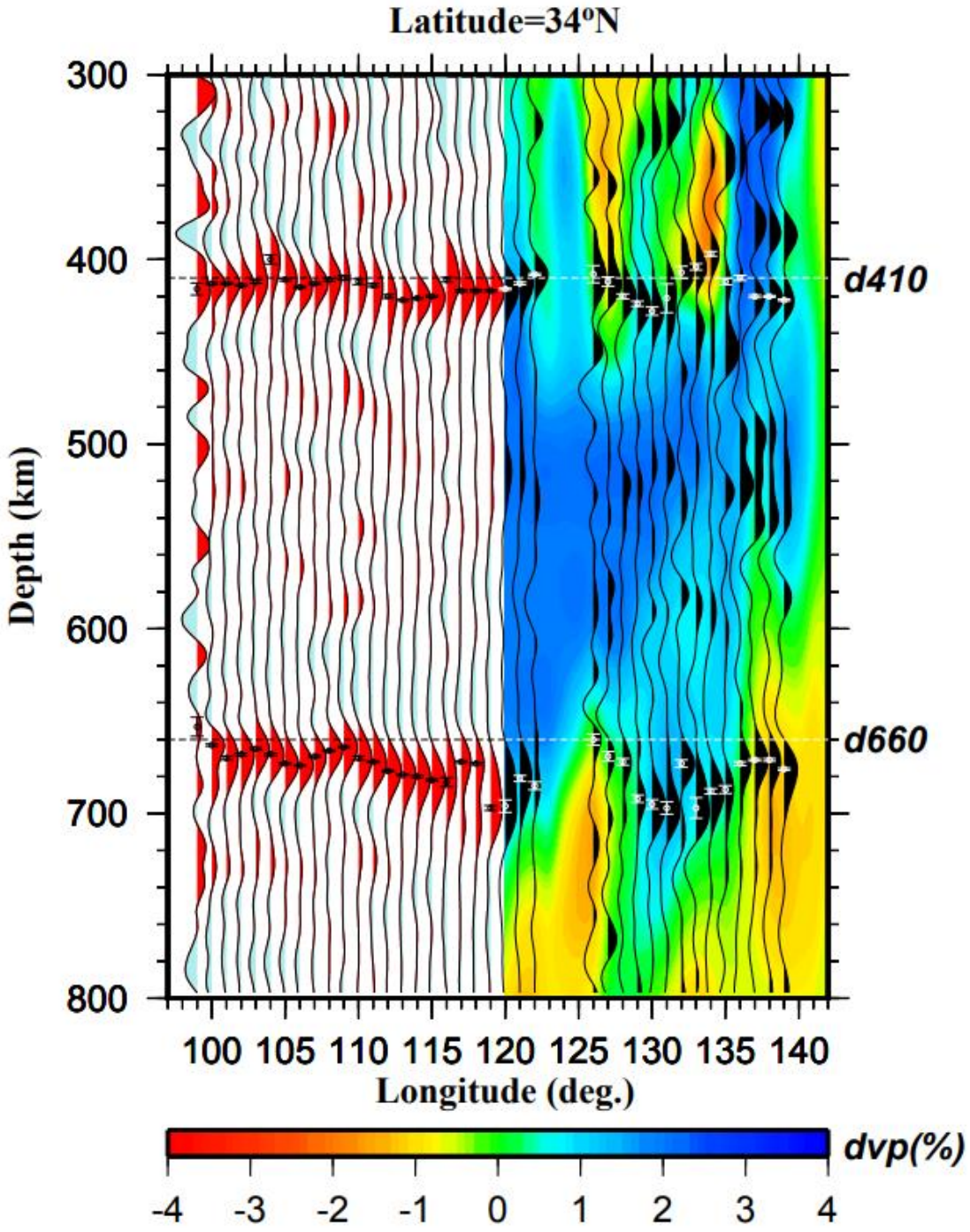

Figure S3. (a) Depth series from stacking of RFs in radius = 1º bins along 34° N latitudinal profile. The background image shows the P-wave velocity anomalies (Chen et al., 2017).

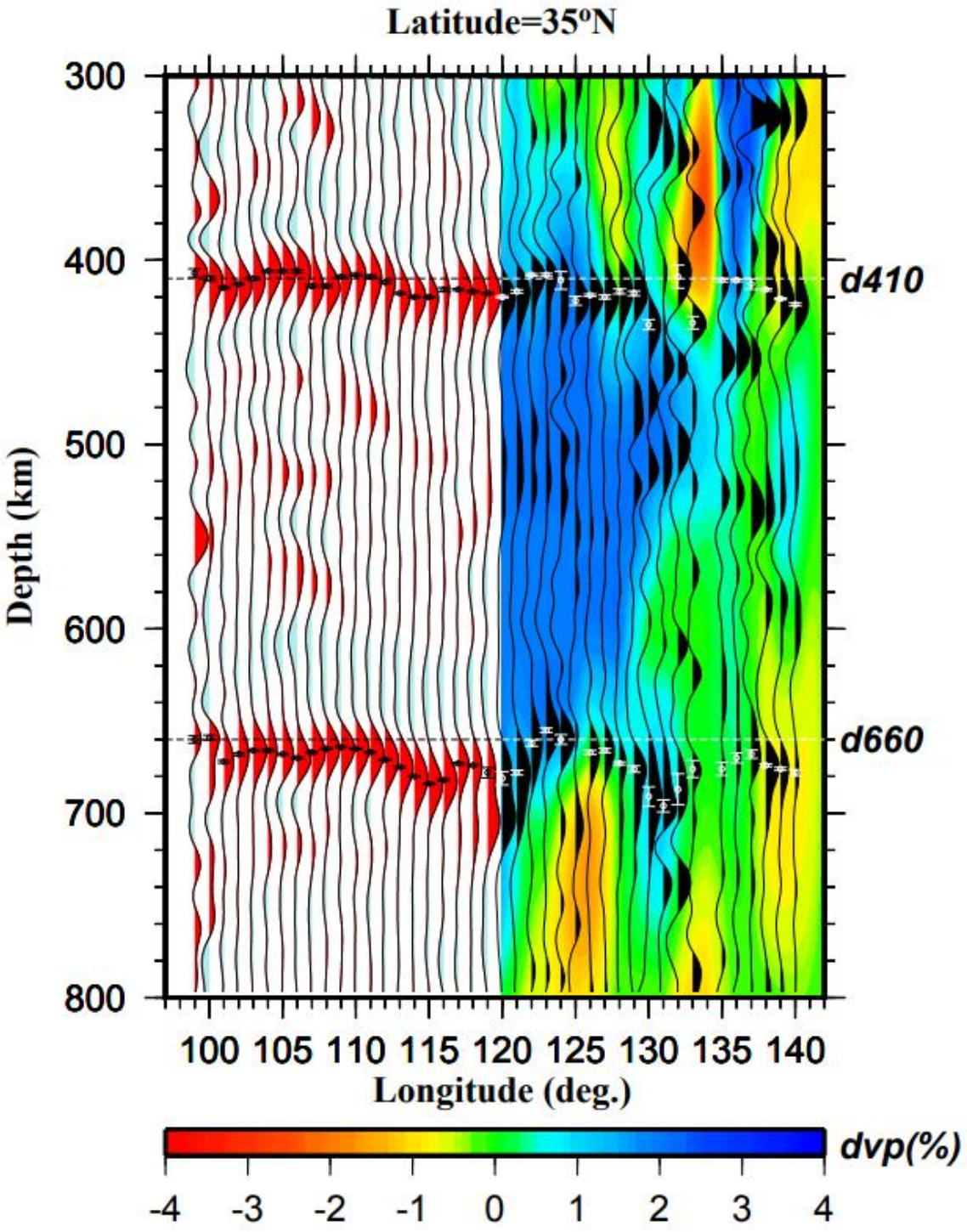

Figure S3. (b) Same as (a) but for latitude 35° N.

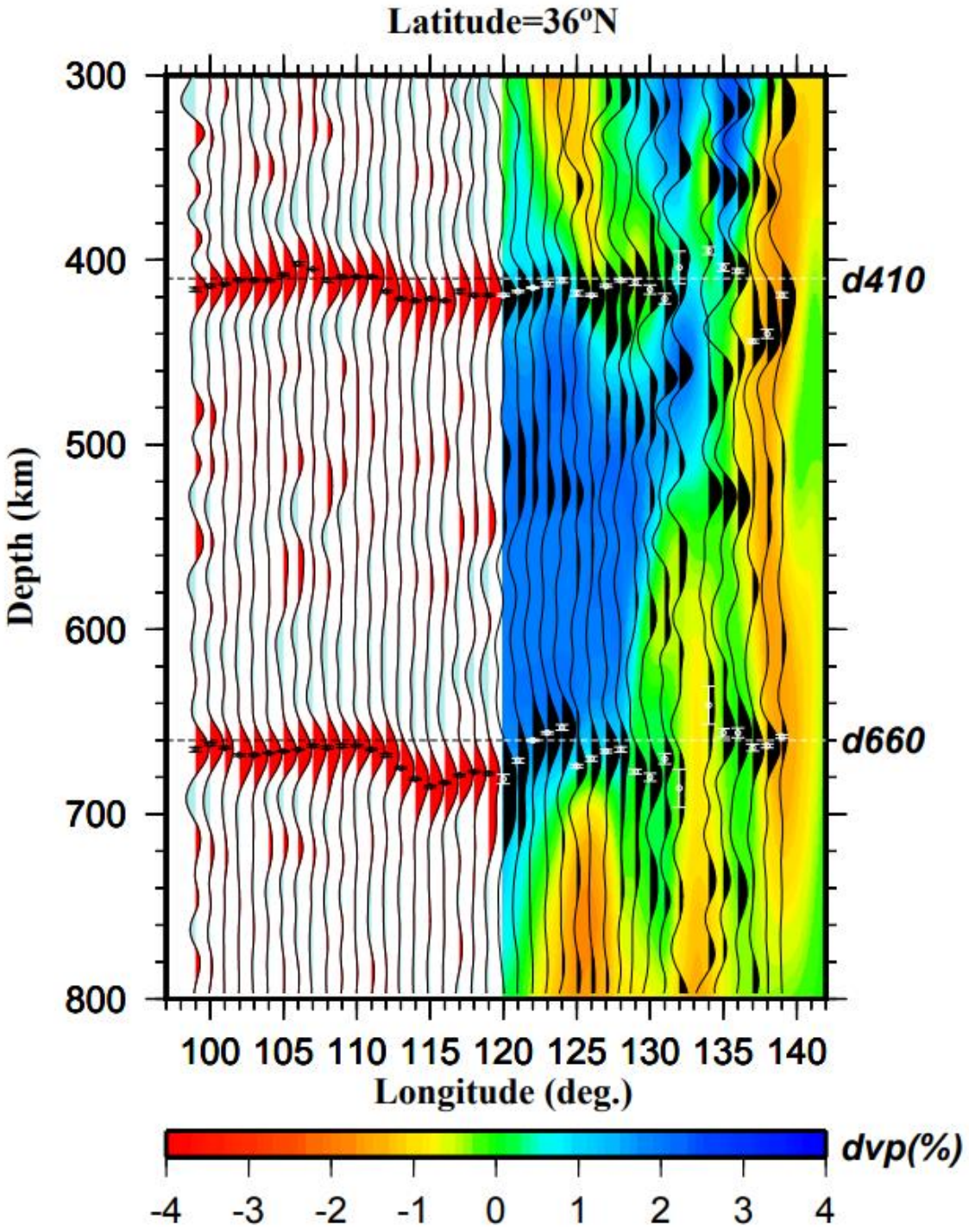

Figure S3. (c) Same as (a) but for latitude 36° N.

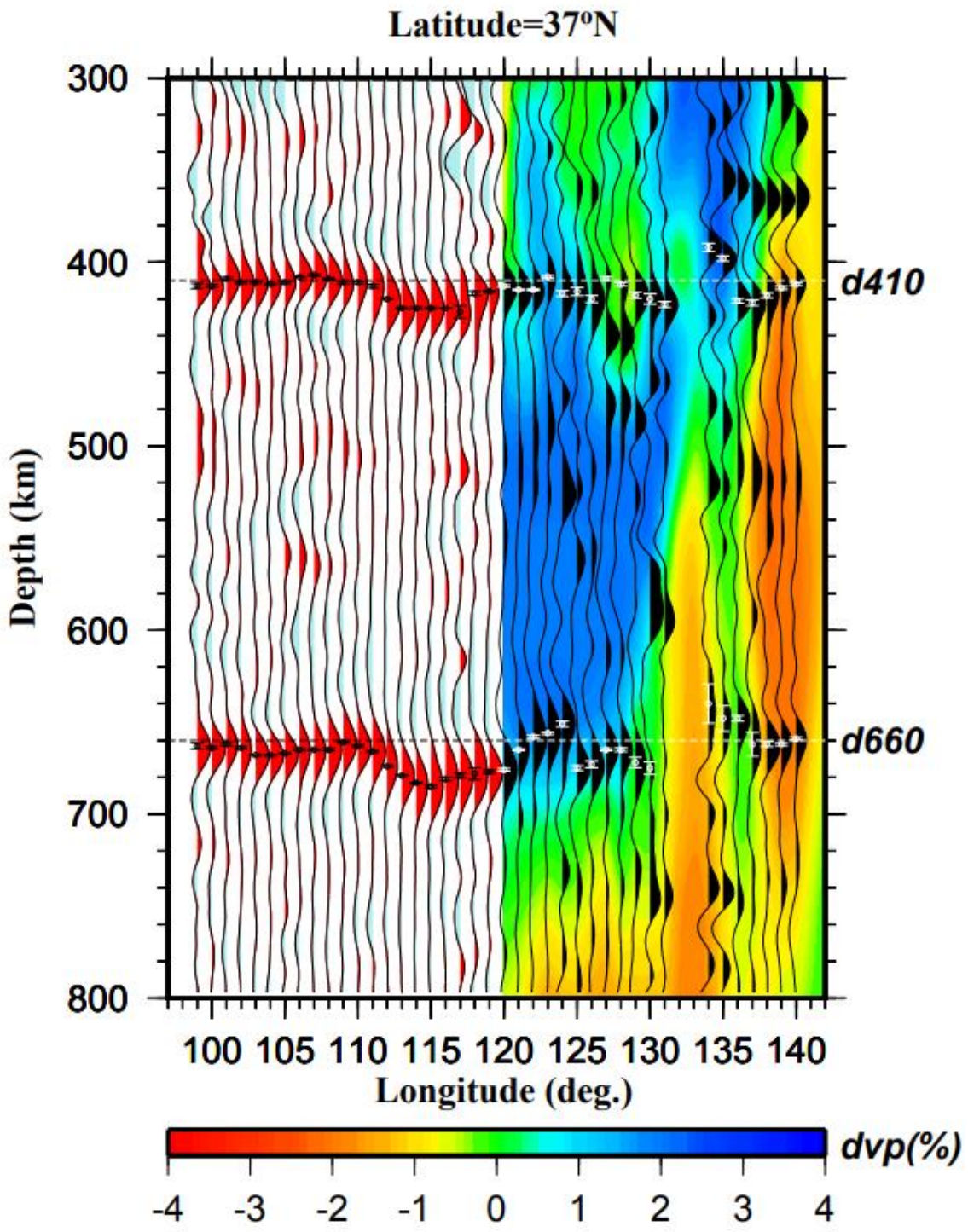

Figure S3. (d) Same as (a) but for latitude 37° N.

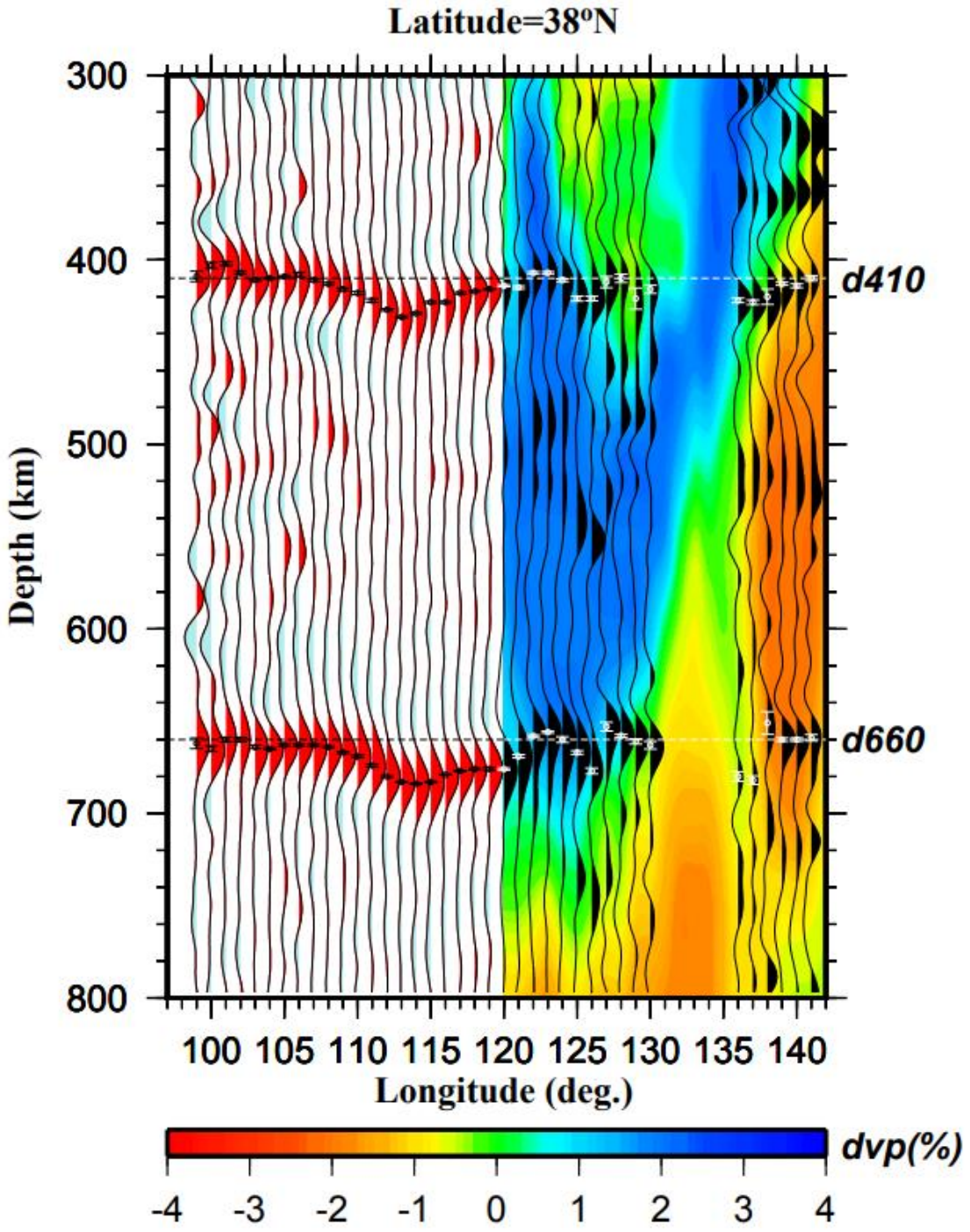

Figure S3. (e) Same as (a) but for latitude 38° N.

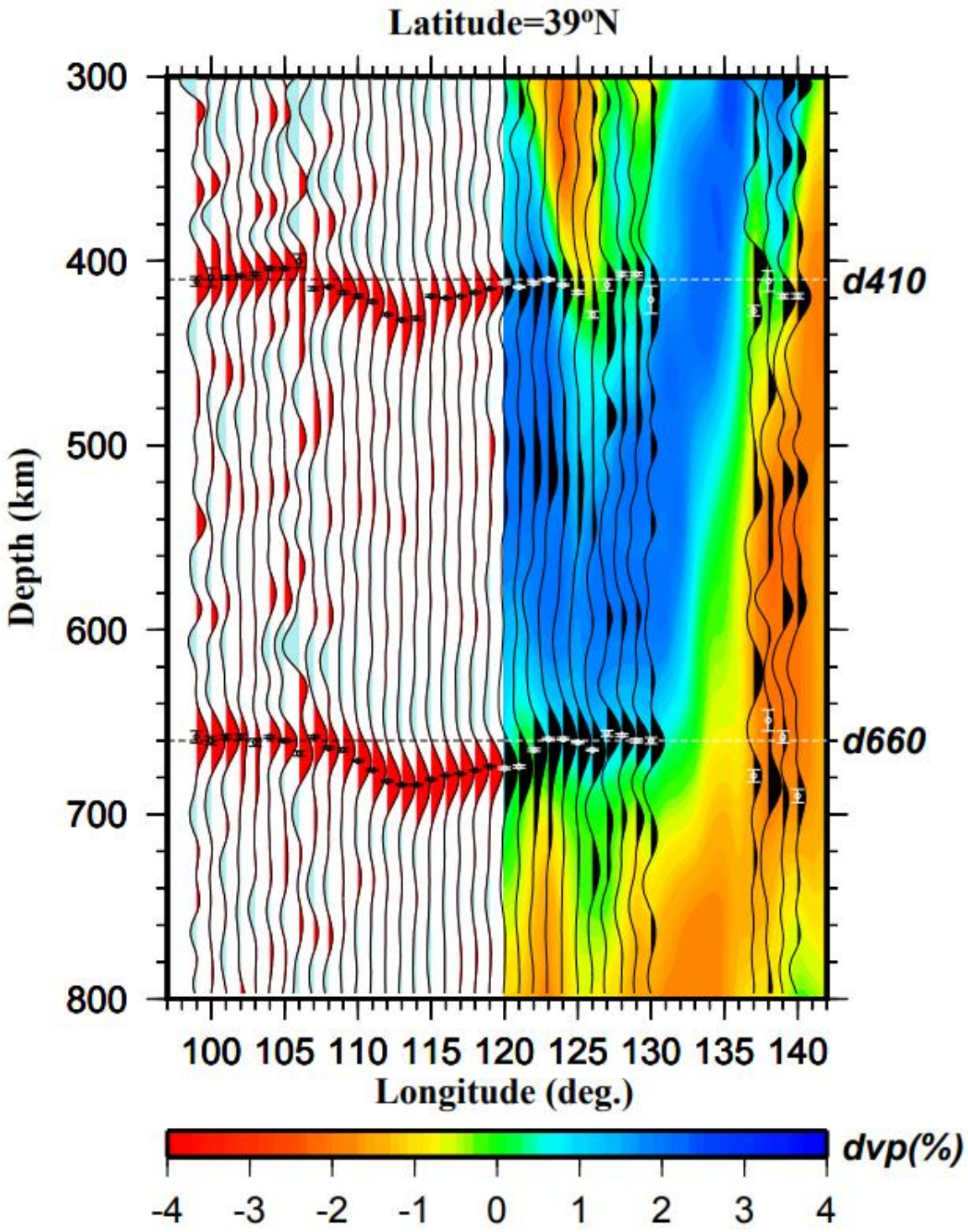

Figure S3. (f) Same as (a) but for latitude 39° N.

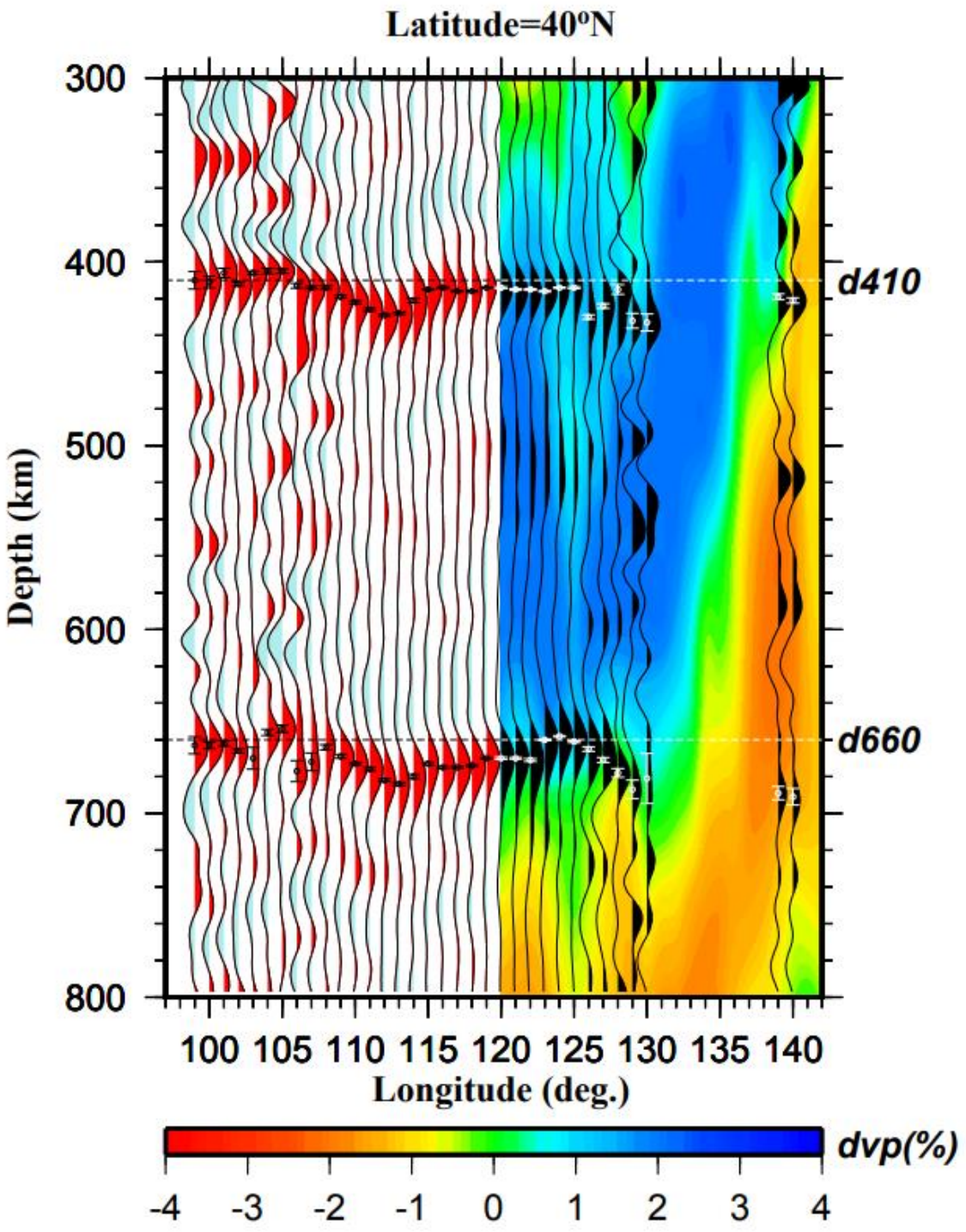

Figure S3. (g) Same as (a) but for latitude 40° N.

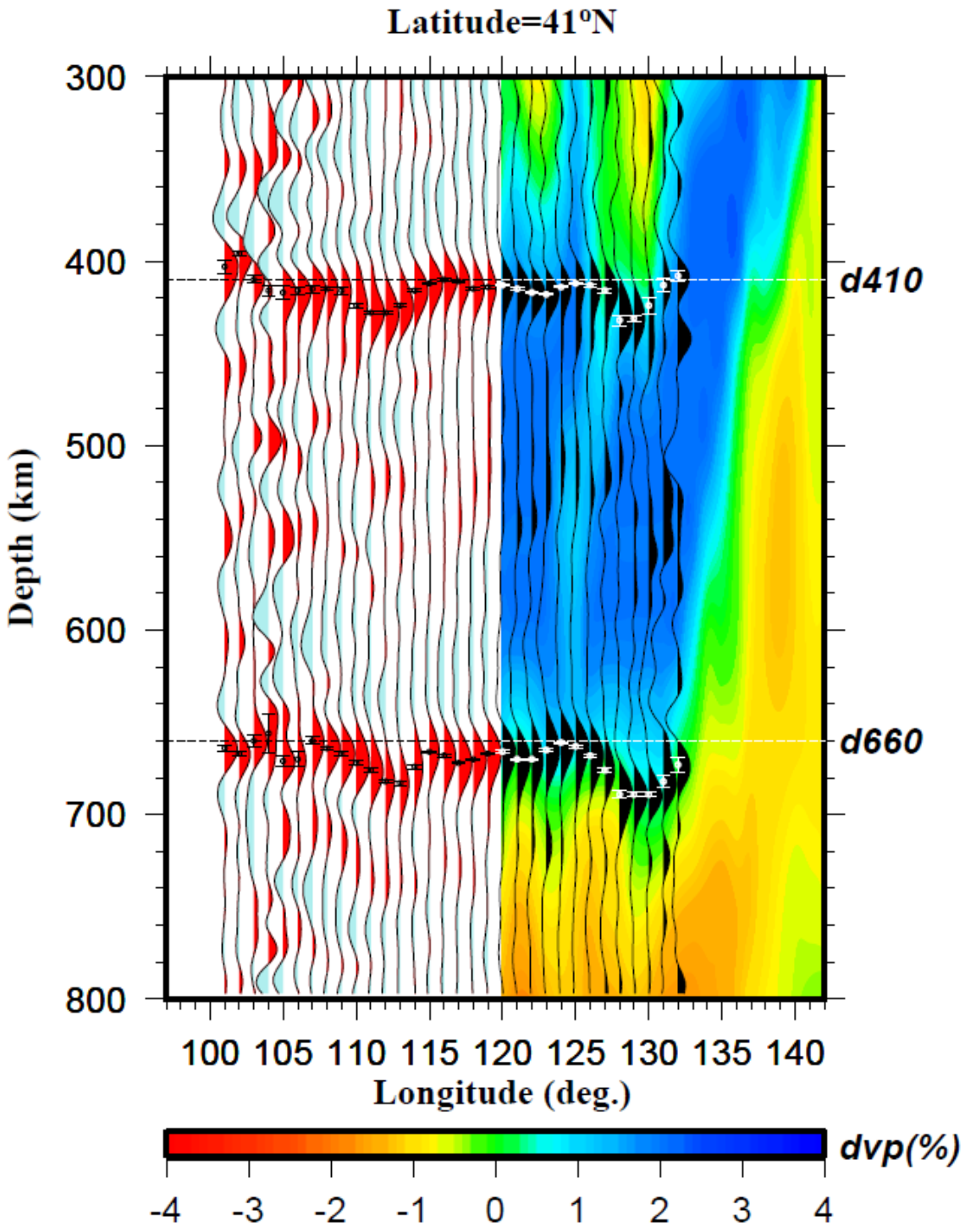

Figure S3. (h) Same as (a) but for latitude 41° N.

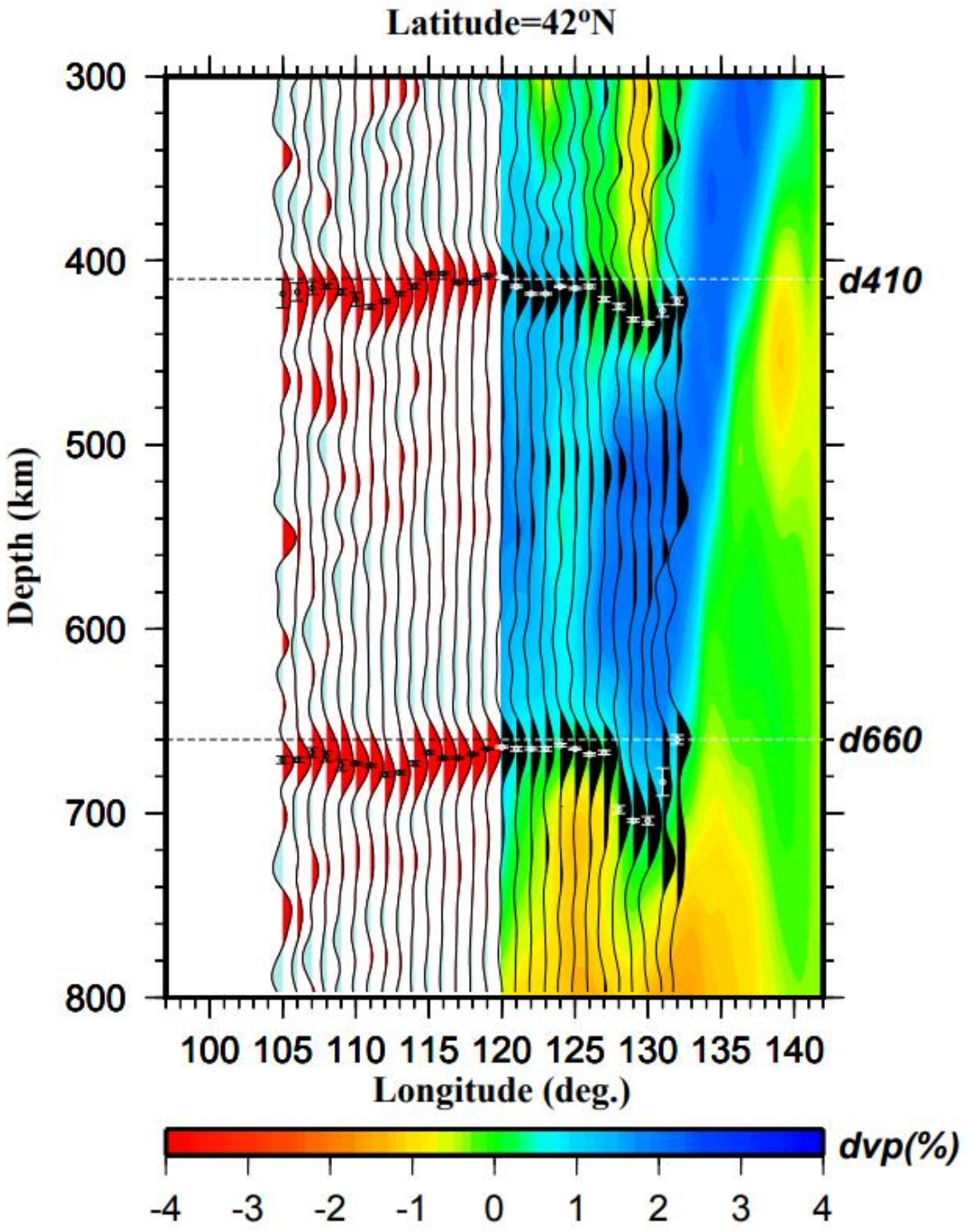

Figure S3. (i) Same as (a) but for latitude 42° N.

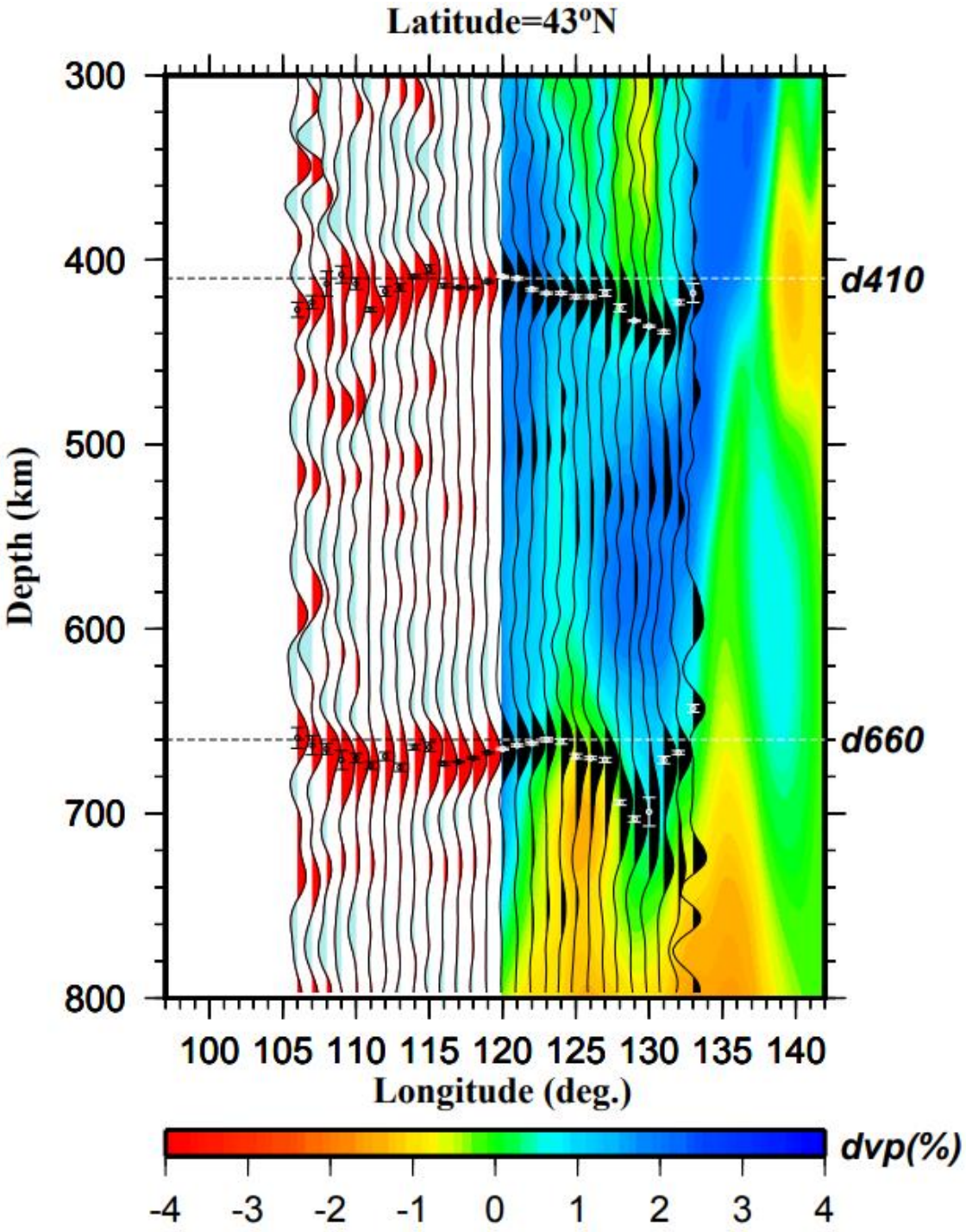

Figure S3. (j) Same as (a) but for latitude 43° N.

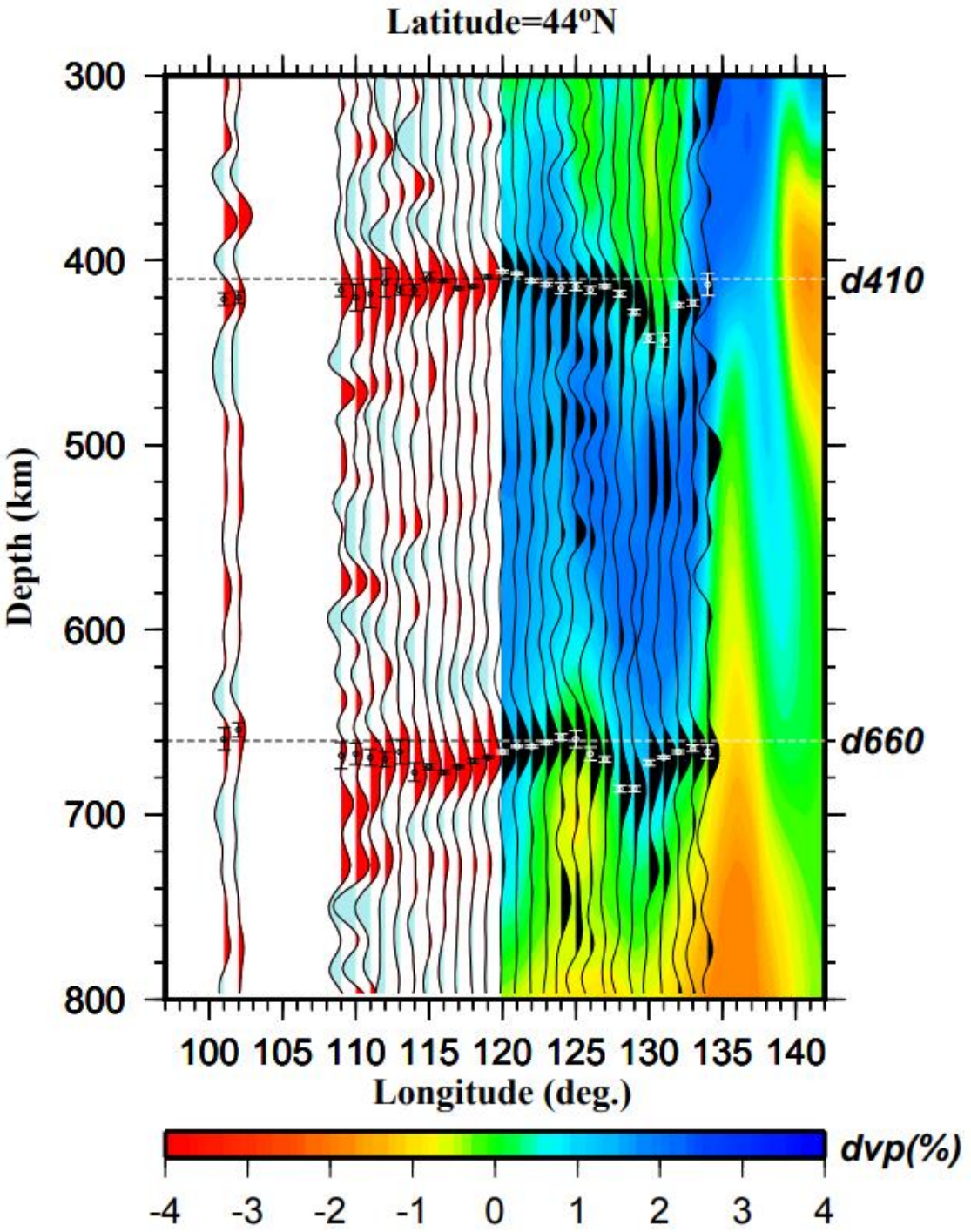

Figure S3. (k) Same as (a) but for latitude 44° N.

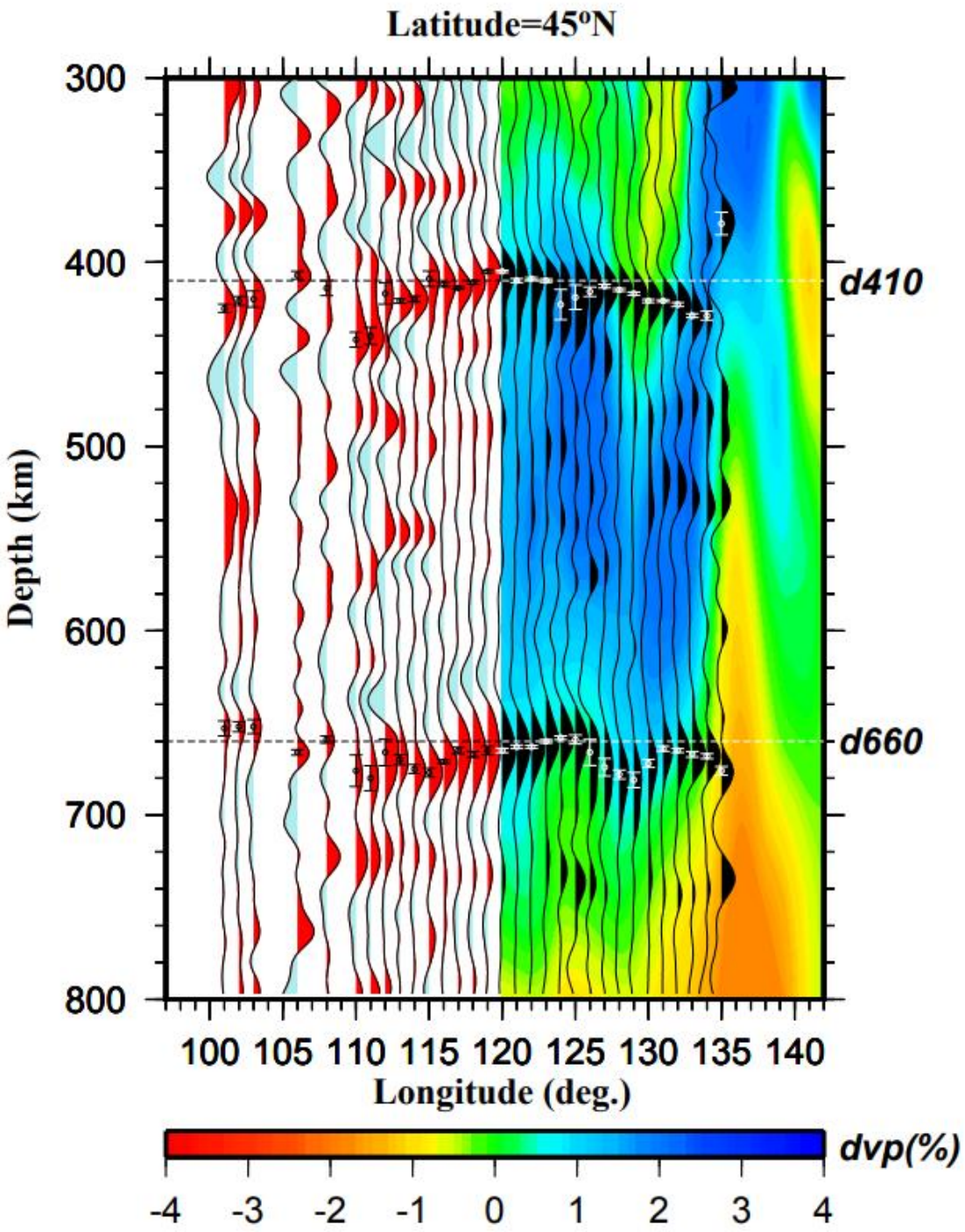

Figure S3. (l) Same as (a) but for latitude 45° N.

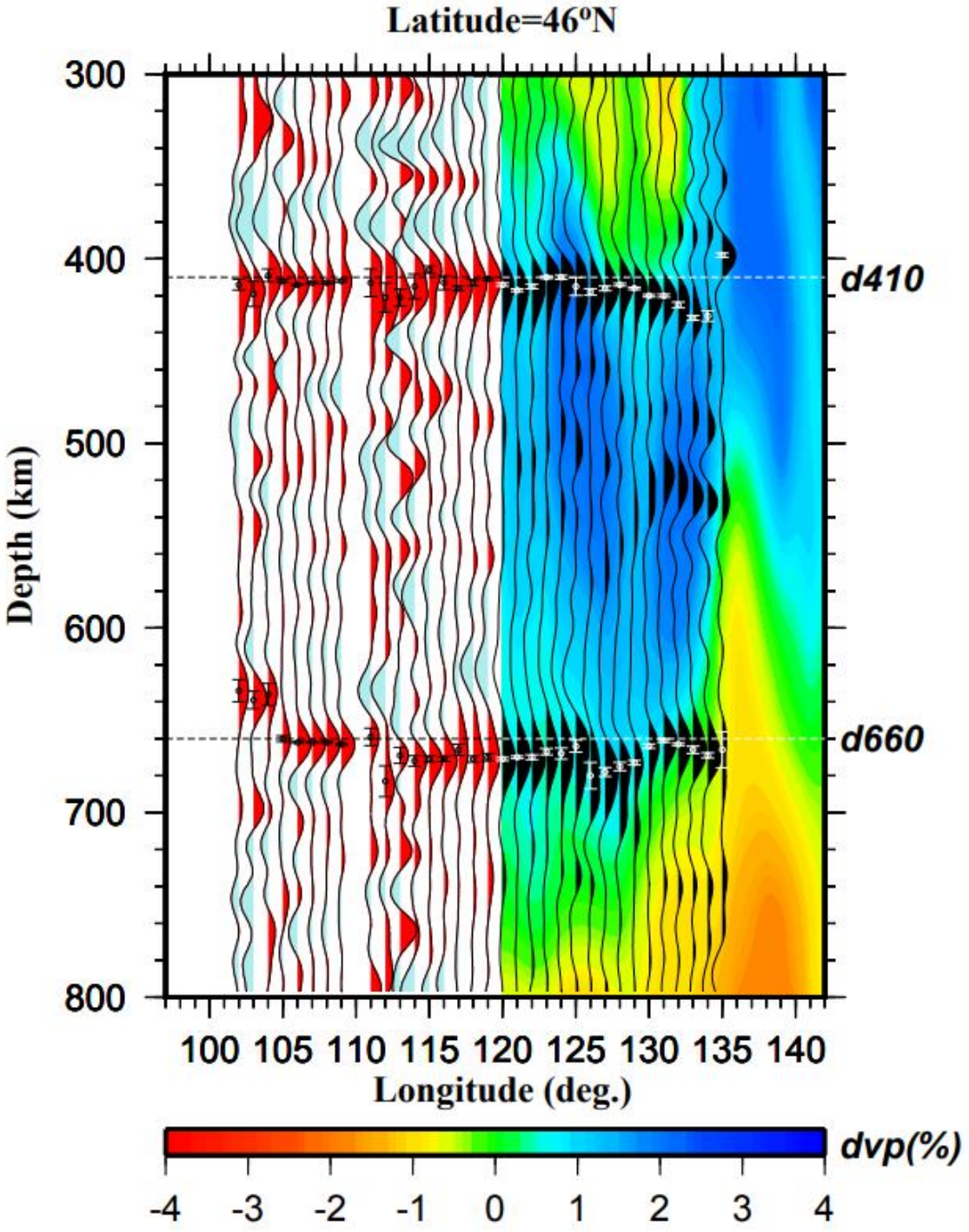

Figure S3. (m) Same as (a) but for latitude 46° N.

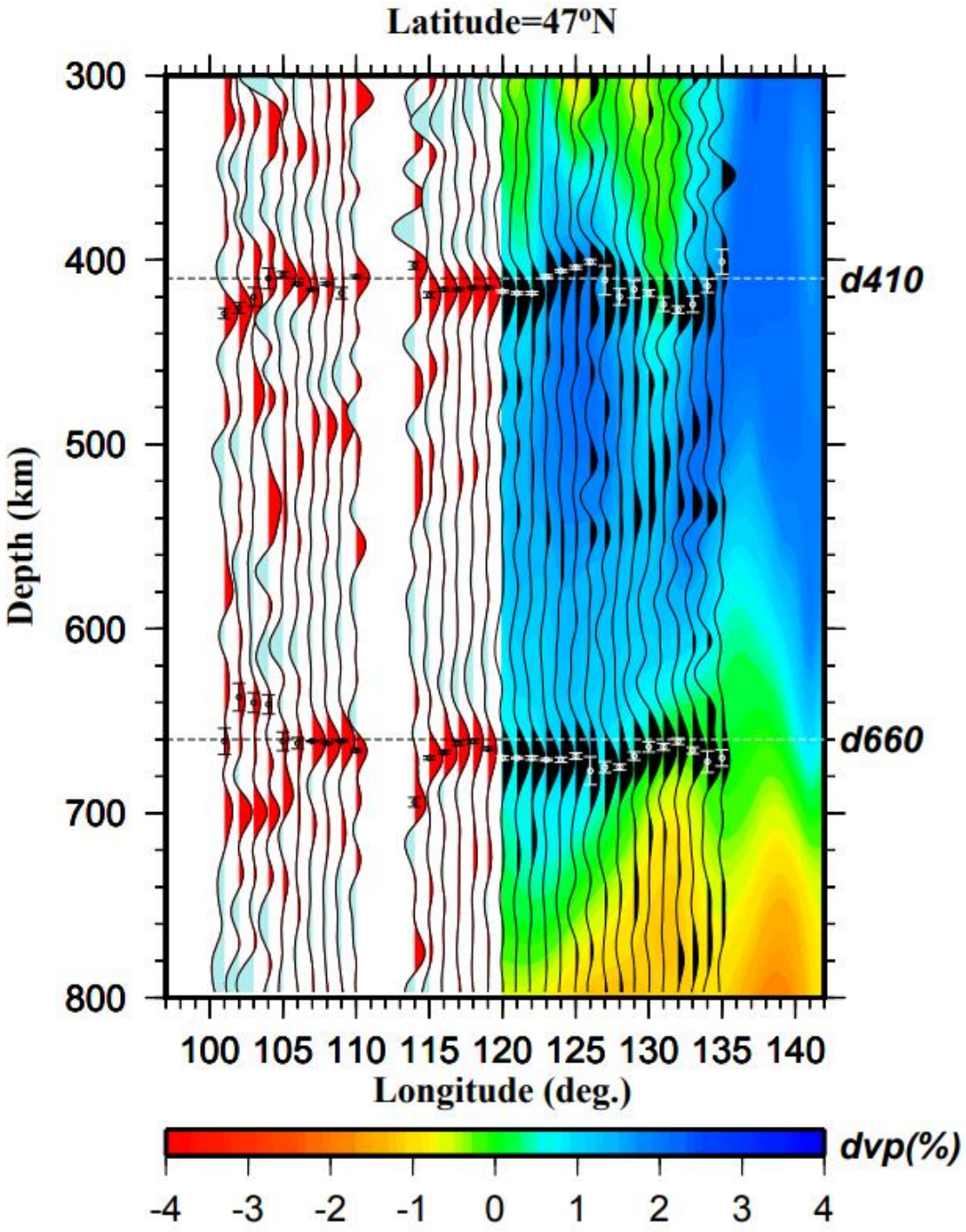

Figure S3. (n) Same as (a) but for latitude 47° N.

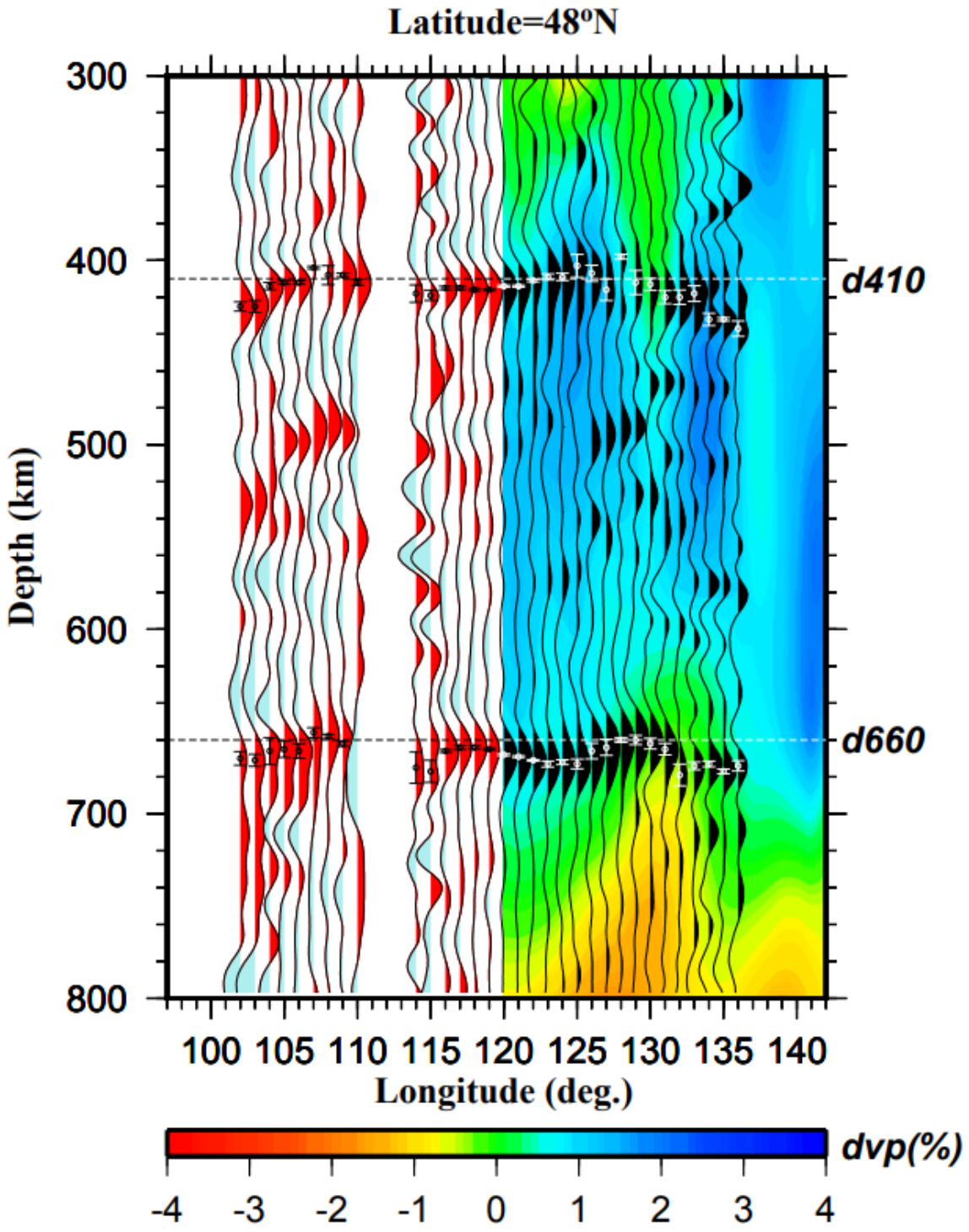

Figure S3. (o) Same as (a) but for latitude 48° N.

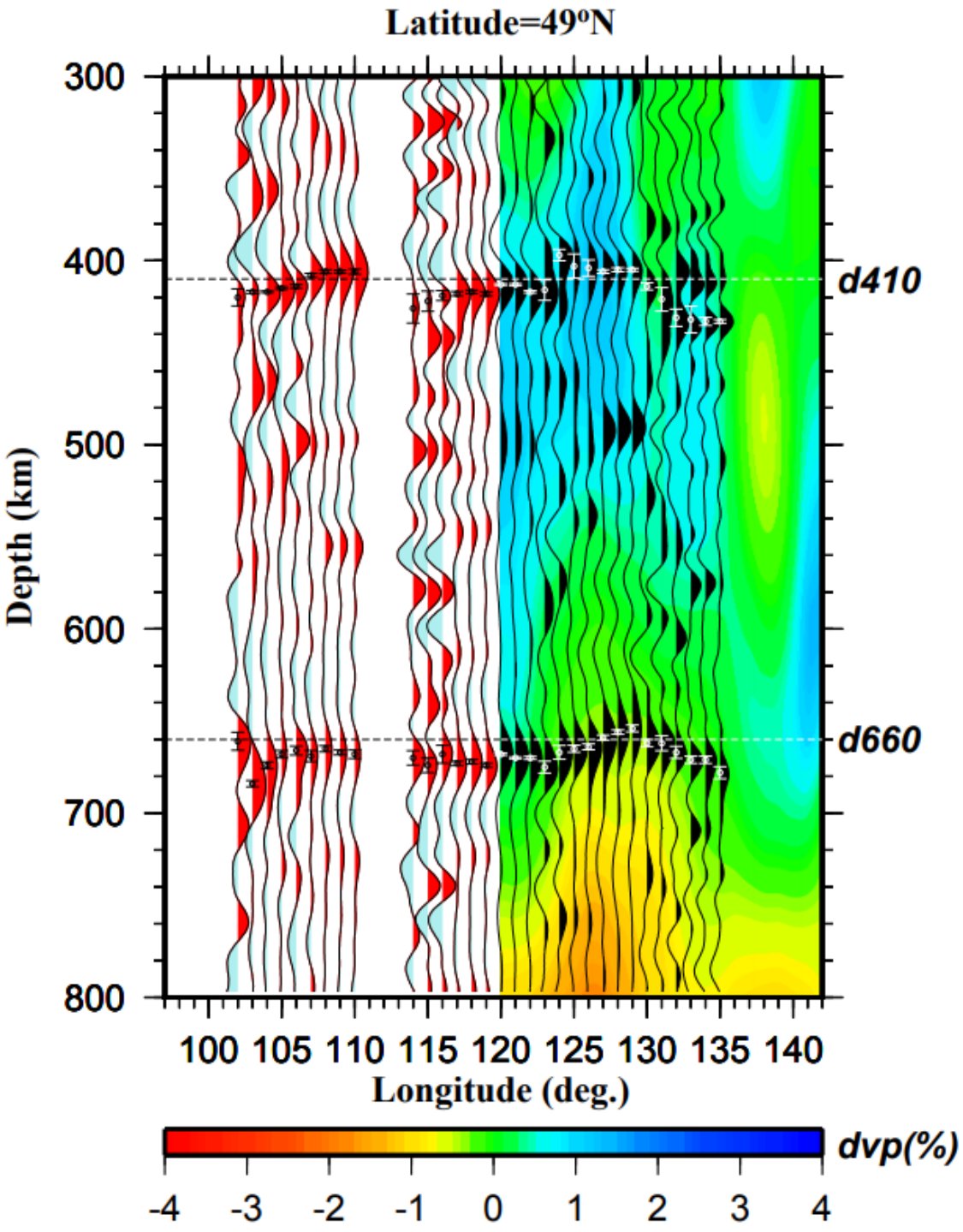

Figure S3. (p) Same as (a) but for latitude 49° N.

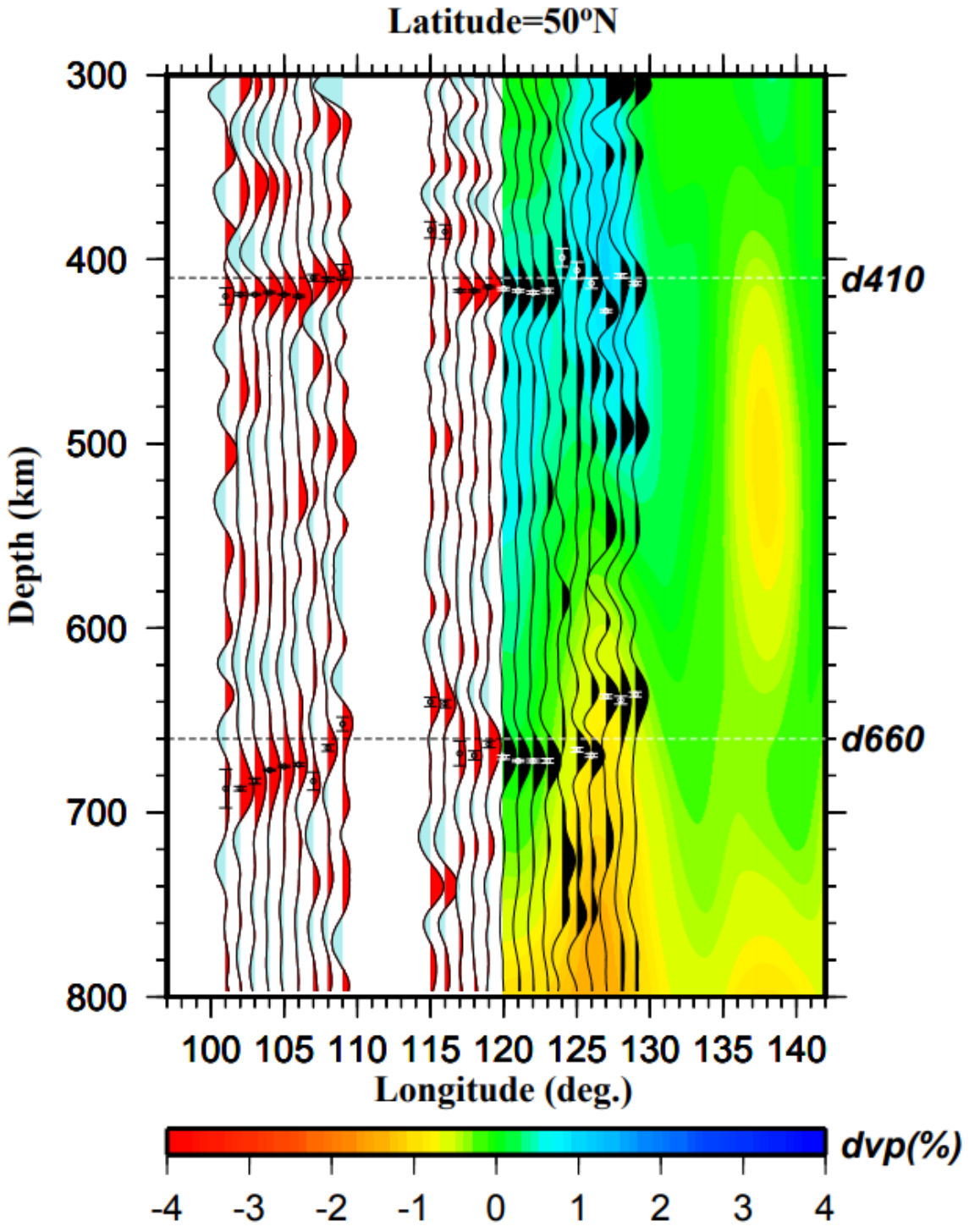

Figure S3. (q) Same as (a) but for latitude 50° N.

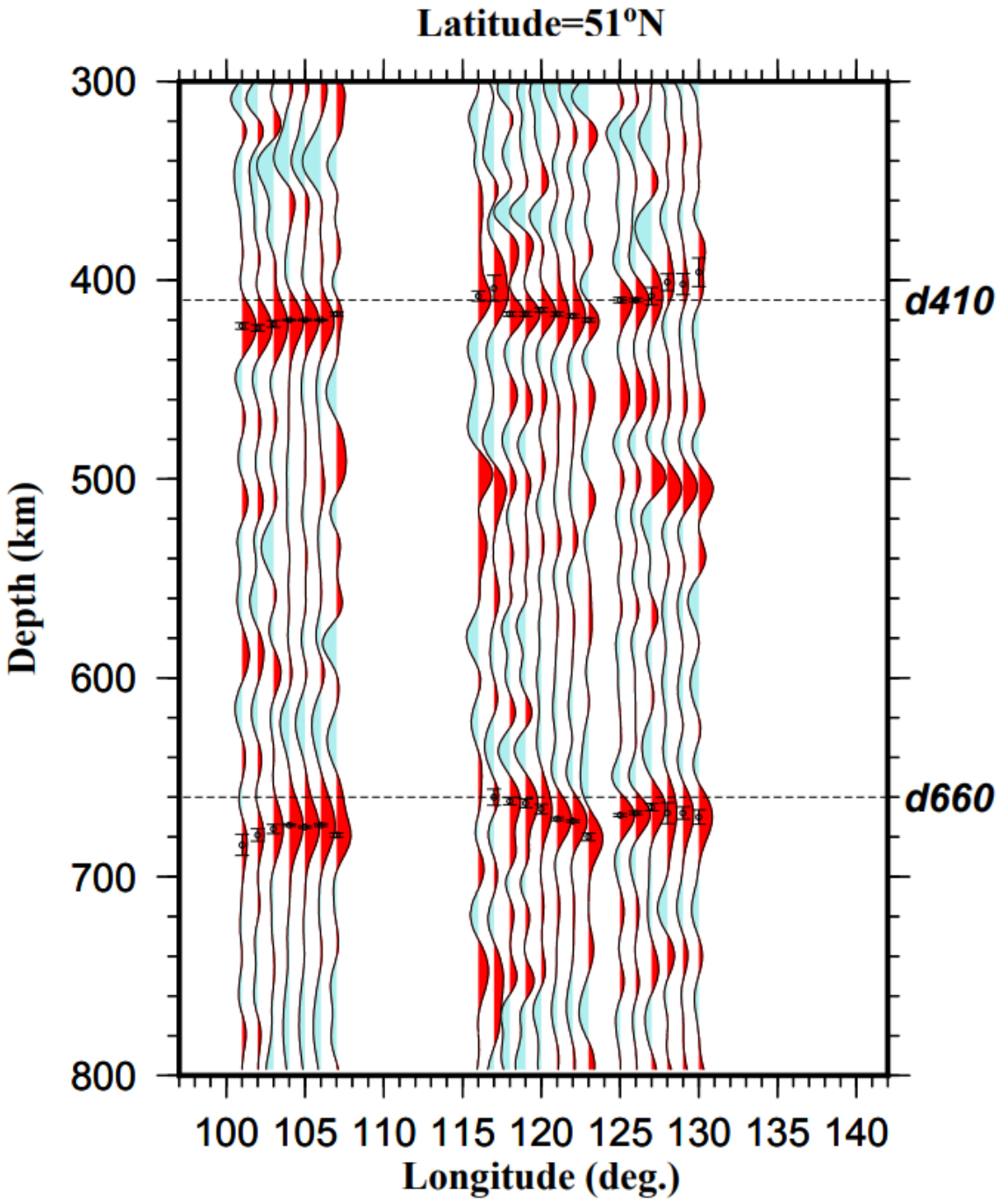

Figure S3. (r) Depth series from stacking of RFs in radius = 1° bins along 51° N latitudinal profile.

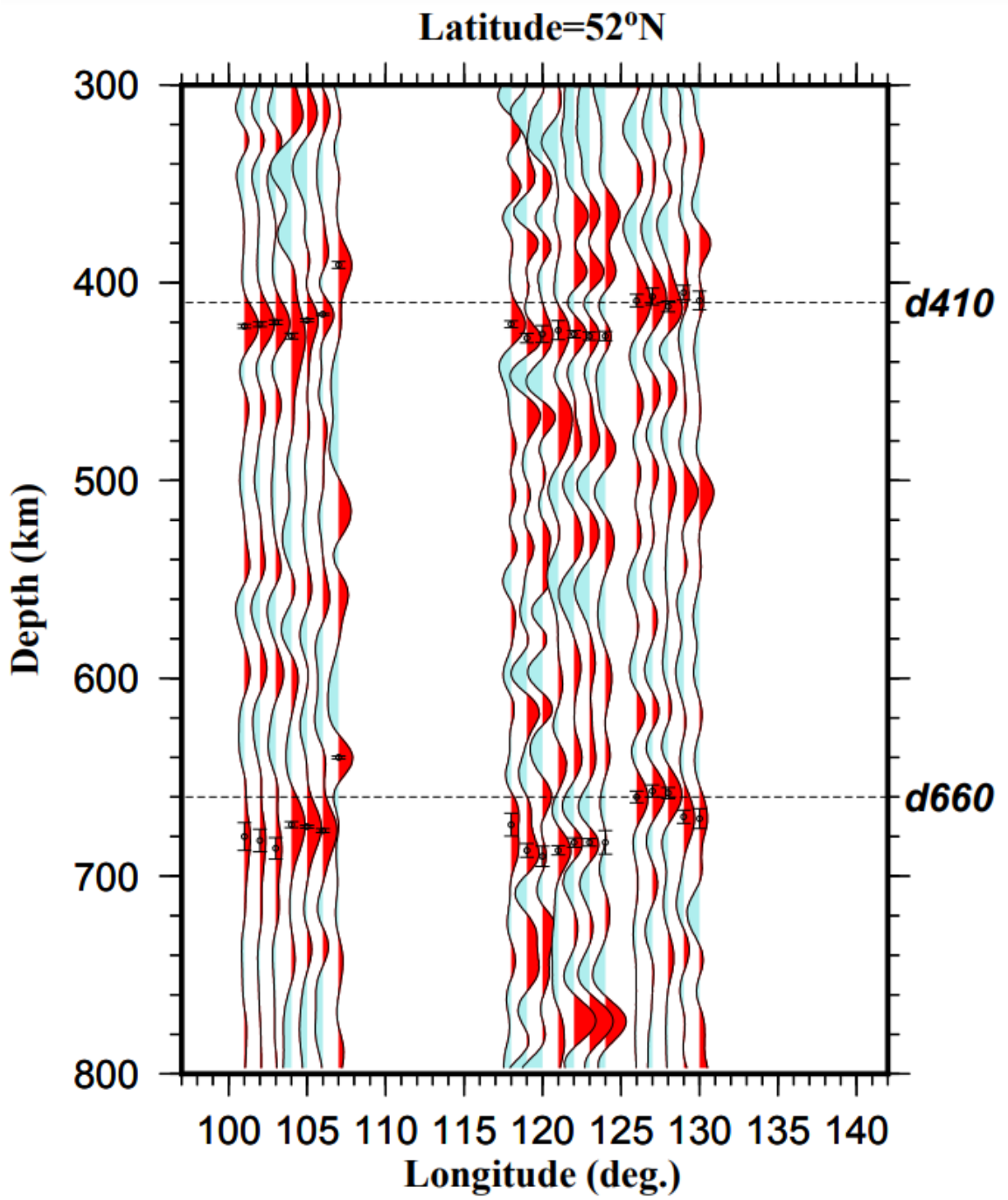

Figure S3. (s) Same as (r) but for latitude 52° N.

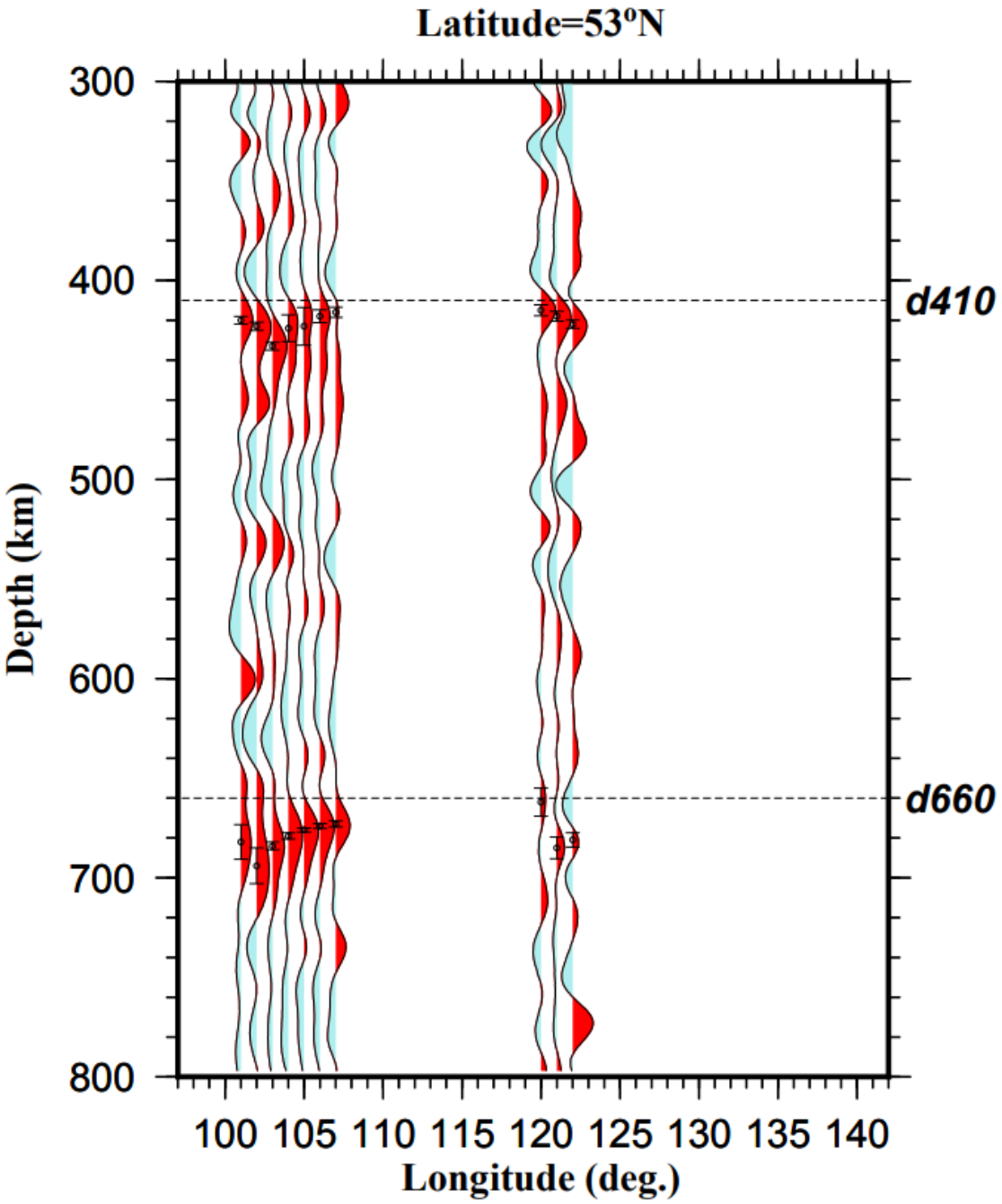

Figure S3. (t) Same as (r) but for latitude 53° N.

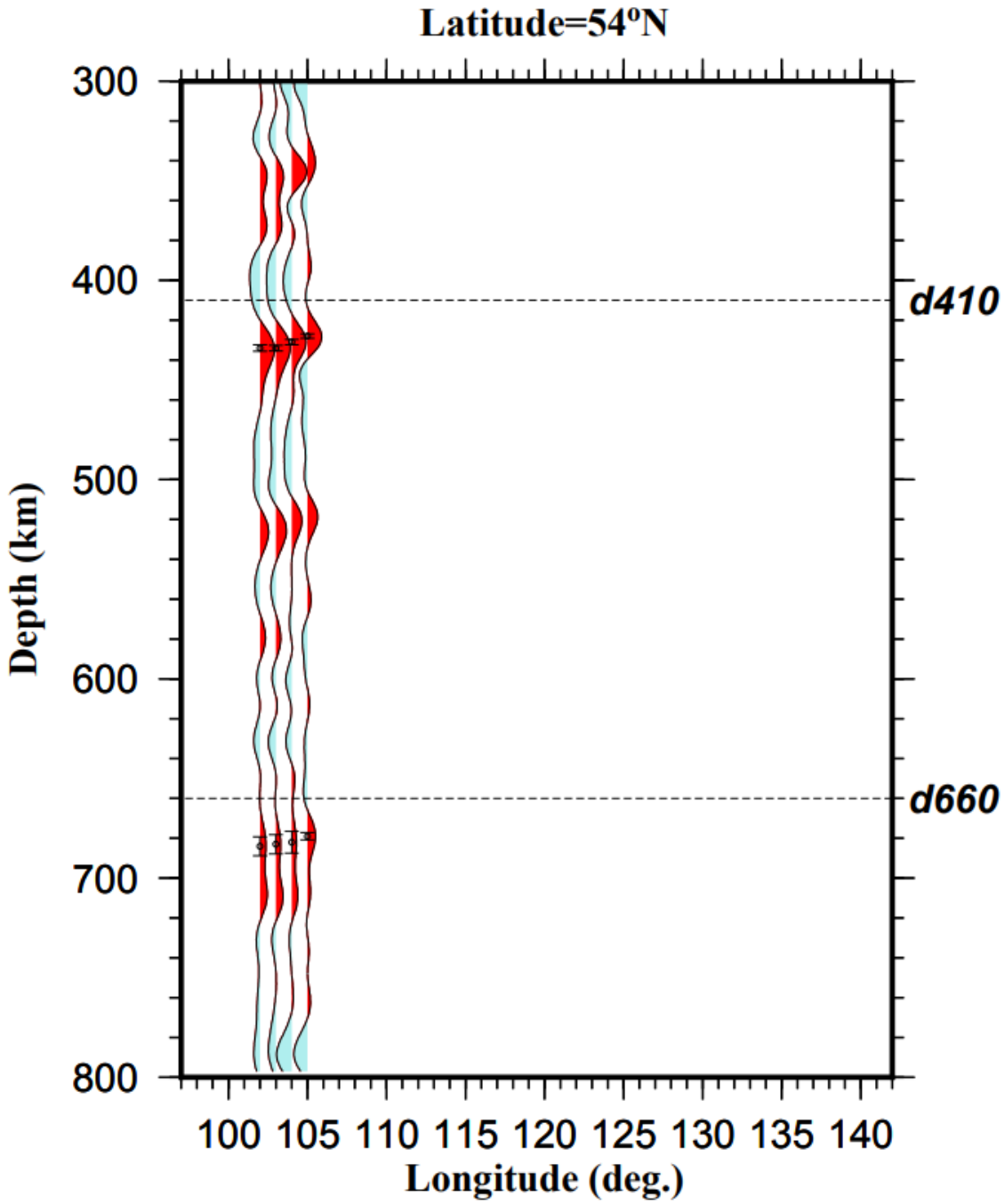

Figure S3. (u) Same as (r) but for latitude 54° N.

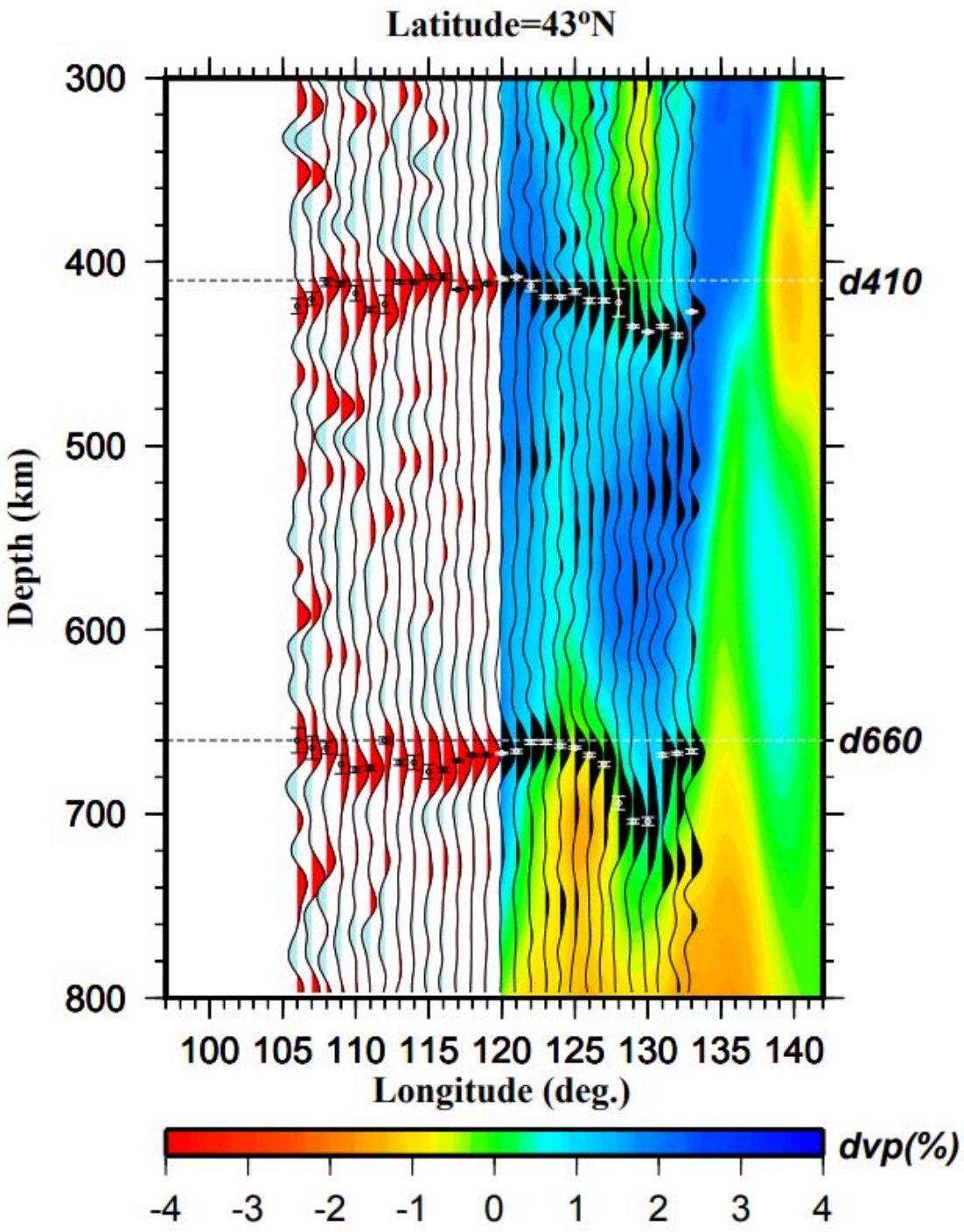

Figure S4. Depth series from stacking of RFs filtered by 0.03 – 0.3 Hz in radius = 1° bins along 34° N latitudinal profile. The background image shows the P-wave velocity anomalies (Chen et al., 2017).

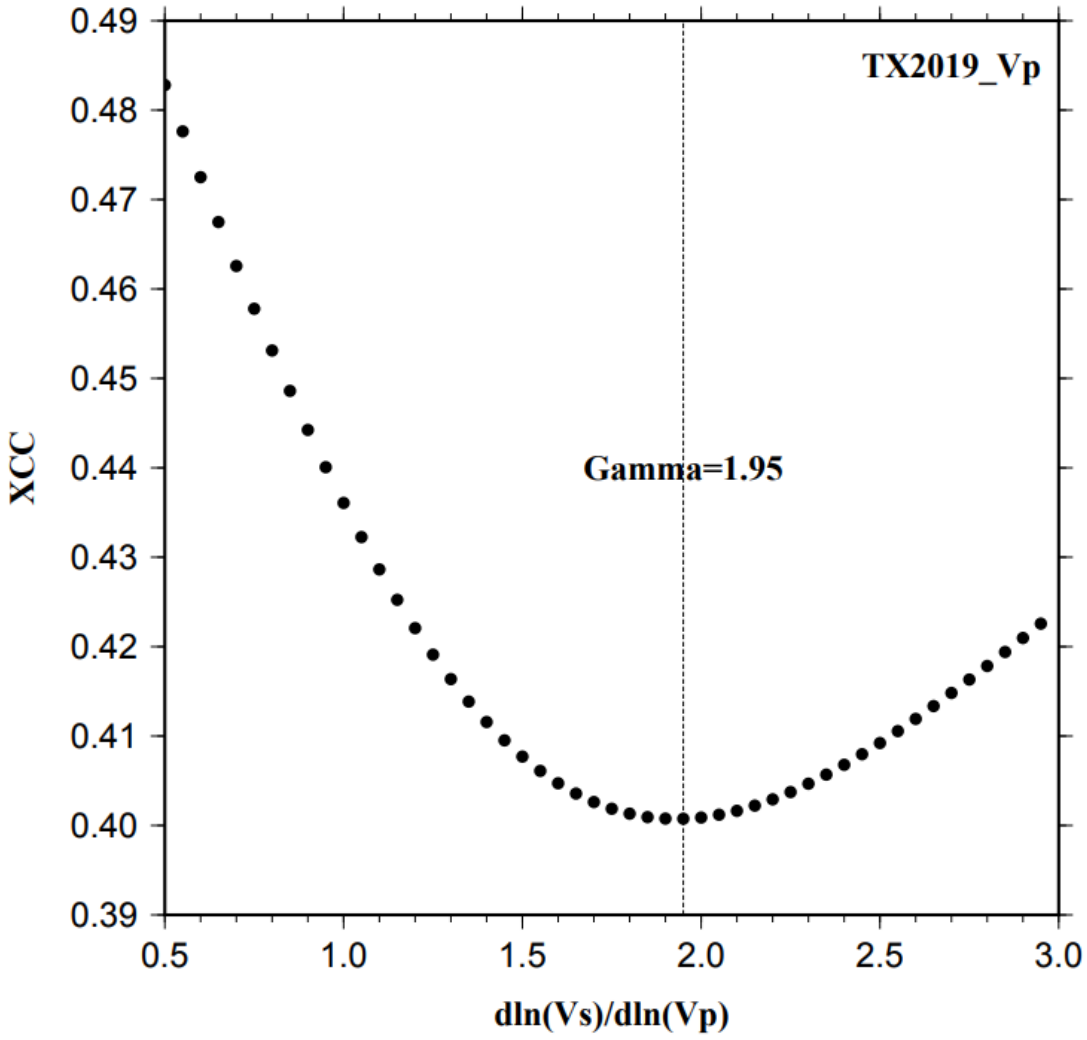

Figure S5. Cross-correlation coefficients between corrected d410 and d660 depths plotted against dln(Vs)/dln(Vp) values using P wavespeed model from Lu et al. (2019) .

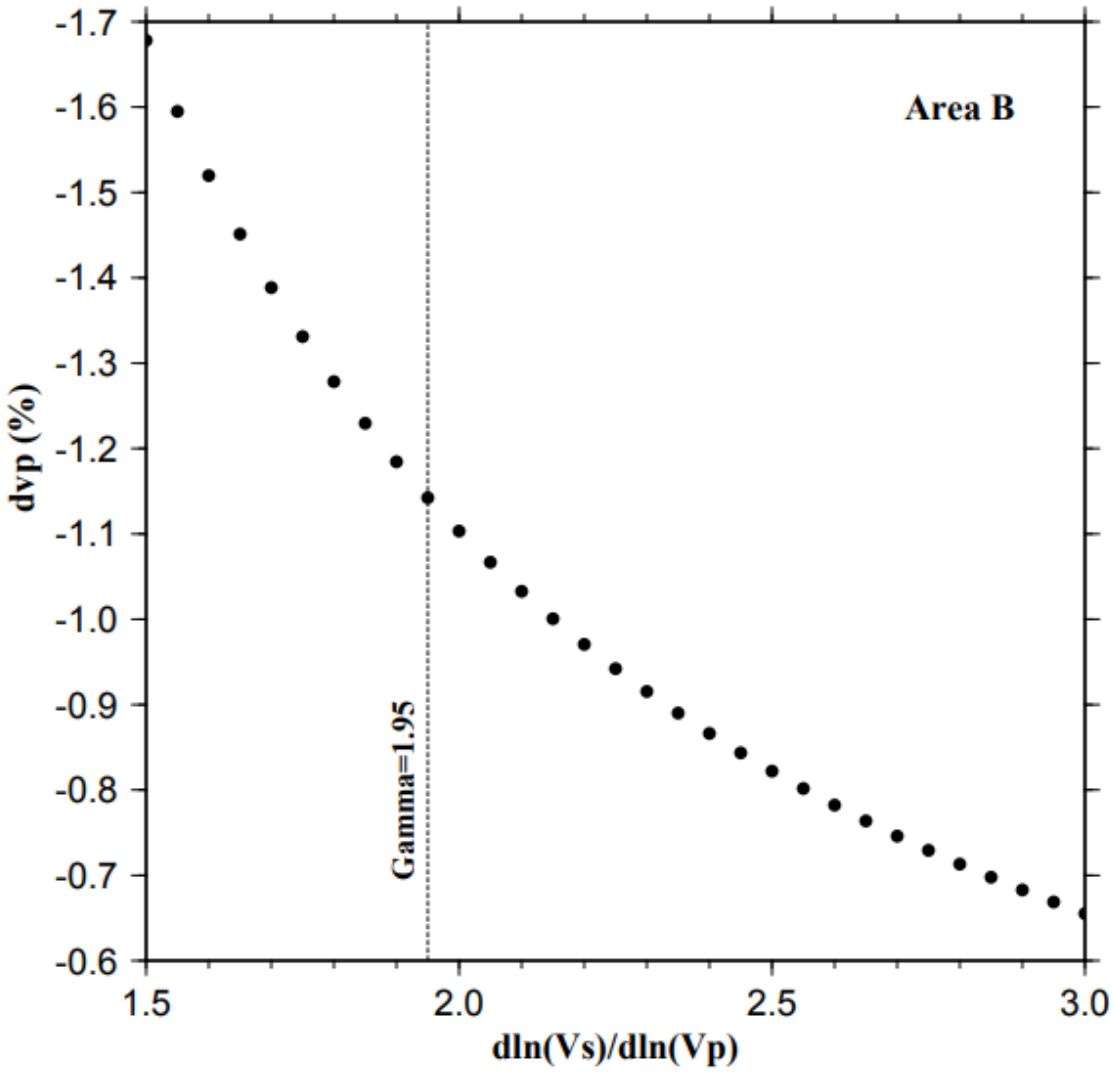

Figure S6. P wave speed anomaly above the d410 plotted against dln(Vs)/dln(Vp) value beneath Area B.